International Journal of Innovative
Computing, Information and Control
Volume **14**, Number **3**, June **2018**

ICIC International ©2018 ISSN 1349-4198
pp. 1015–1028

PEAK BRACKETING AND DECREMENTED WINDOW-SIZE SCANNING-BASED MPPT ALGORITHMS FOR PHOTOVOLTAIC SYSTEMS

Faizal Arya Samman[1,*], Abdul Azis Rahmansyah[2] and Syafaruddin[1]

[1]Department of Electrical Engineering
Faculty of Engineering
Universitas Hasanuddin
Kampus Gowa, Jl. Poros Malino Km.6, Bontomarannu 92171, Indonesia
*Corresponding author: faizalas@unhas.ac.id

[2]Department of Power Engineering
Politeknik Bosowa
Jl. Kapasa Raya No.30, Tamalanrea, Makassar 90241, Indonesia

Received July 2017; revised December 2017

Abstract. *This paper presents a peak bracketing algorithm and a decremented windows-size scanning-based algorithm to trace a maximum power operation point of a solar array in photovoltaic systems. Power curves of the systems can contain some local maximum power points, besides a global maximum power point (MPP). This problem appears due to the existence of partial shadows or non uniform solar irradiance on the photovoltaic panel surfaces. Atmospheric condition changes (irradiance and temperature changes) can also change the power curves and MPP locations on the curves. Three types of the iterative scanning-based MPPT algorithms are proposed to solve the partial shading problem and the changes of power curves, i.e., decremented window scanning, peak bracketing (PB) method and PB with initial scanning. The simulation results have presented that, for some cases, those MPPT algorithms can find out the global maximum power points (MPPs) of the partially shaded photovoltaic system with relatively smaller number of perturbing-and-observing (P&O) steps. The proposed algorithms can significantly outperform a traditional hill-climbing method in terms of the number of required P&O steps to reach the global MPP.*

Keywords: Power electronics, Maximum power point tracking algorithm, Photovoltaic systems, Renewable energy, Partial shading problem

1. **Introduction.** Renewable energies have become promising energy sources in the near future for industries and human life. For some decades ago, fossil fuels have been used as the main energy resources for industries, transportation and many other human life mobility and activities. Air pollution caused by the excessive use of fossil fuels due to rapid industrial growth, as well as the decreased amount of fossil fuel resources is main reasons of a new campaign to use renewable energies. Renewable energies such as solar energy, wind, tidal, wave, geothermal energy, bio-ethanol and biomass are among potential energy sources, which can be optimally used in the future.

The primary energy resource in the earth is the sun (solar energy). By using a solar cell (photovoltaic cell), the irradiation of solar energy can be converted into electric energy. The solar cells arrangements will form a solar module. The solar modules can be arranged to achieve a solar panel. A solar array in $N \times M$ structure can be further obtained by utilizing the solar panels. Every form of solar array will have different power curve characteristics, which depend on the configuration and the size of the solar array. Moreover,

the technology used to manufacture the solar cells and external working environment can also affect the solar array power characteristics.

The current technologies used for solar cell manufacturing have unfortunately a drawback. As the open circuit voltage of the solar output terminal is higher, then energy loss will happen, because some parts of energies are transformed into thermal energy instead of electric energy. Therefore, the electric current will be reduced, while the thermal energy increases. Thus, the power will also be dropped accordingly. Fortunately, at every different solar array installation and environmental condition, there is a voltage point, where the solar system operates at its maximum (peak) power point. The maximum power delivery can be achieved continuously by maintaining the solar system output voltage to operate at this expected point.

A photovoltaic system that supplies power to alternating current (AC) loads and direct current (DC) loads is presented in Figure 1. The main discussion domain of this paper as presented in the figure is the maximum power point tracking (MPPT) module. This is an important part of a charge controller unit. In the MPPT module, a specific MPPT algorithm is embedded, which is used to control the solar system in such a way that it will always operate at its maximum power point. This paper will discuss and propose algorithms to maintain solar power operation at the peak point. The proposed algorithm is named as peak bracketing and decremented windows-size scanning, which require lower number of scanning steps to find the expected maximum power point during normal and partial shading conditions.

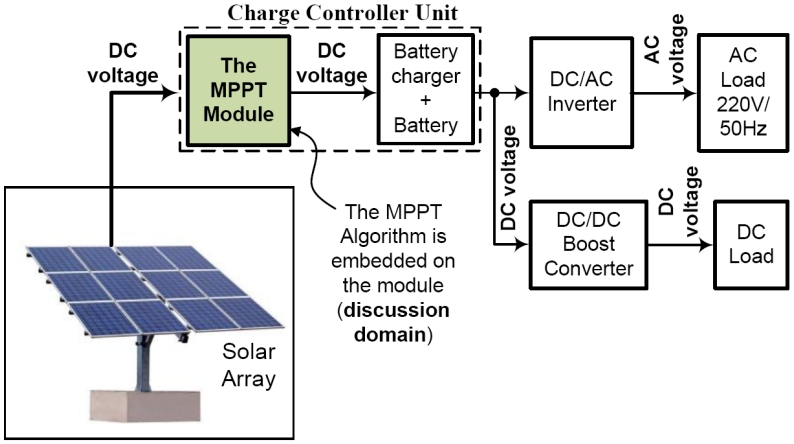

FIGURE 1. Photovoltaic-based home-scale power system generation with DC and AC transmission

Since most of renewable energies produce DC power, including the photovoltaic cells, then DC power lines would be interesting electric installation for future homes. The standard DC voltage should be determined for future implementation, such that all consumer electronic producers can set the DC input terminal voltage of their products to follow the standardized voltage. Nevertheless, this issue is not further discussed in this paper.

The remaining sections of this paper are organized in the following. Some literature papers related to our current research and the contribution of this paper are explored in Section 2. The system architecture and the simulation setup are presented in Section 3. Section 4 discusses the simulation results for some different resistance loading conditions and shading scenarios. Finally, the conclusion and a few outlooks for further system development are presented in Section 5.

2. **Related Works.** Some techniques or methodologies to realize an MPPT algorithm are presented in literature. The techniques for examples are perturb and observe (P&O) technique [1, 2, 3, 4], P&O hill climbing method, incremental conductance [5], fractional open-circuit voltage, fractional short-circuit current, fuzzy logic method, neural-based method, ripple correlation control [6], back-stepping sliding mode control [7] look-up table techniques, one-cycle control technique, and feedback of power variation techniques [8]. An extreme seeking control method is another technique that is closely related to the ripple correlation control method and P&O method [3, 9].

A general problem in the applications of solar power generation is partial shading (partial shadow). Some particular techniques are proposed to overcome the problem, which are designed directly in the considered MPPT algorithms [10, 11, 12]. A power curve characteristic of a solar array with a partially shaded surface is presented in Figure 2. When partial shadow caused by, e.g., cloud shadows is partially applied to the solar array panel surface or materials deployed uniformly on the solar surface, a few local maximum power points (MPPs), besides a global MPP, will probably appear at the power curve.

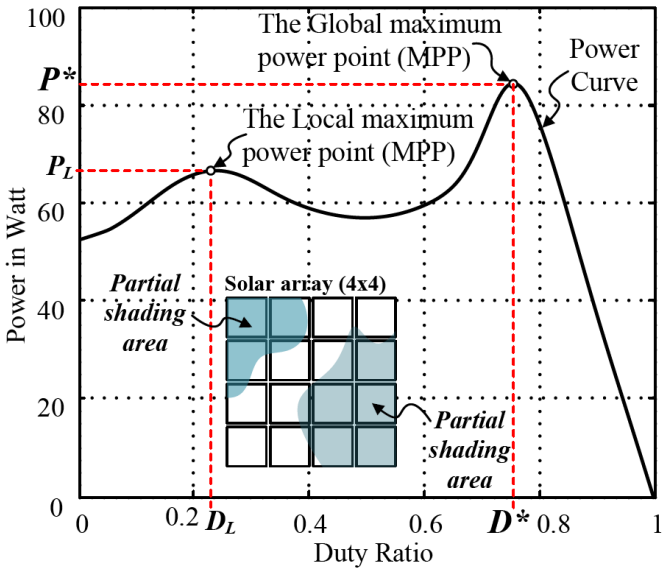

FIGURE 2. Power curve characteristic of a partially shaded solar array

Fractional short-circuit current [13], fractional open-circuit voltage and look-up table techniques are simple but cannot cover well the partial shading problem. The work in [11] attempts to improve the traditional fractional open-circuit voltage (V_{OC}), which states that the expected voltage V^* that delivers a maximum power is located at $0.8V_{OC}$. The method predicts and corrects the expected voltage V^* by using a set of equations. However, this method neglects the load conditions. The change of loads can significantly change power curves. When load changes are involved by the work in [11], more complex prediction equations will be needed. Since load conditions are not predictable in practice, then the set of requested equations will be infinity. In contrast to the above method, our proposed algorithms do care about the load changes with no extra program coding. In other words, the problem has been implicitly taken care in the existing MPPT control algorithms.

Some non-conventional or artificial intelligence (AI) techniques can also be used to overcome the partial shading problem. A few of them are, e.g., fuzzy logic, neural-based approaches and particle swarm optimization (PSO) method [14] or combination of them with P&O method [15], with scanning and store algorithm [16], and fuzzy-PI method

optimized with genetic algorithm [17]. Once shading condition measurement values are co-related with memorized conditions, the AI method can find fast the expected power point. The AI techniques, unfortunately, require pre-study of the solar array configuration [6]. By using fuzzy logic techniques, base knowledge about the solar array should be achieved previously. In the MPPT algorithm using neural-based techniques, the MPPT module and solar arrays should be pre-trained in advance with large number of training data. The training data are obtained from the pre-study of the solar array configuration. Although genetic algorithm can be used to optimize the fuzzy method performance, an extra optimization computing will increase the complexity and computing cost of the MPPT algorithm.

The most used MPPT technique to solve the partial shading method is P&O technique. The P&O techniques do not require such base knowledge and pre-training. The P&O techniques used in our algorithms operate based on decremented step-size duty-ratio scanning or duty-ratio perturbation. Our approach is similar to the work in [18], but the difference is based on the used perturbing signal. Generally speaking, a perturbing signal can be made in the form of duty ratio of a pulse signal applied to the gate of a power MOSFET in the DC/DC converter, perturbing current and perturbing voltage. The work in [18] uses current subject as the perturbing signal, while our proposed algorithms use duty-ratio as the perturbing signals. Our proposed MPPT algorithms, which are divided into 3 algorithms namely decremented-window-size scanning (DWS), peak bracketing (PB) and PB with initial scanning (PBIS) algorithms, fall into the class of P&O method as the improvement of traditional P&O hill climbing method. Our proposed MPPT algorithms can accelerate the global MPP finding. The P&O hill climbing method uses a very simple approach, but it can potentially be locked at a local maxima.

In our proposed MPPT algorithms, the power is measured at the output terminal of the DC/DC converter. Therefore, a voltage and current sensor are installed at the terminal. The multiplication of both sensor signals will produce a power signal. This is the main unique design approach of our proposed MPPT techniques compared to existing MPPT methods. Many research works measured the power from the solar array terminal such as in [2, 4, 10, 12, 18, 19, 20]. The maximum power points of the power curves measured from the solar array output and the converter output will not always be at the same duty cycle point. Based on our specific consideration, we prefer to choose the power measurement from the converter output, since this power is more actual for the users point of view. Moreover, the current at the solar array output has ripple whose frequency is high and equal to the switching frequency for the used DC/DC converter. This ripple causes a bad current sensor operation. It can shorten the sensor lifetime and induce extra switching power losses.

3. **The Algorithms and Simulation Setup.**

The photovoltaic system discussed in this paper consists of a photovoltaic array, a boost-type DC/DC converters and an electronic control unit (ECU). The output voltage and current at the solar output terminal or at converter output terminal are observed after perturbing the DC/DC converter with a pulse waveform having a certain duty ratio. A specific algorithm, embedded on the ECU, is then required to find the best perturbing duty ratio in such a way that the solar system reaches a global MPP. Regarding the partial shading problem, this algorithm should not bring the system working in the unexpected local MPP. The descriptions of the proposed iterative scanning-based algorithms and the simulation setup is described in the following subsections.

3.1. **The MPPT algorithms.** This section describes the proposed MPPT algorithms, which operate using the P&O methods. Each MOSFET gate of the DC/DC converter is perturbed with a pulse signal having D percent of duty cycle. After a few cycle time, the output power of the system is observed. The techniques to find the best perturbing duty cycle D^*, which delivers the expected global peak power point, are presented in the following subsections.

3.1.1. *Decremented window scanning (DWS).* The decremented window scanning (DWS) algorithm traces the global maximum power point of the photovoltaic system by reducing the range of the scanning domain for each iteration. The scanning domain is related to the duty cycle percentage of the pulse signal for the DC/DC converter. While its co-domain unit is the converter's output power in Watt. For N_D number of scanning points, then the same N_D number of domain segments is achieved. A segmented domain, whose maximum power point is in its range, is then selected as the new decremented or smaller size scanning domain. By iteratively finding and reducing a new segmented scanning domain, the best perturbing duty cycle D^*, which gives a global peak power point P^*, will be finally found.

3.1.2. *Peak bracketing (PB).* The peak bracketing (PB) algorithm traces the global maximum power point by bracketing the peak power point with three duty cycle points, i.e., a left duty cycle and power point (D_L, P_L), a right duty cycle and power point (D_R, P_R), and a center duty cycle and power point (D_C, P_C). A bisection method can be used to reduce the tracing domain, or to bracket a higher and higher power point inside a new smaller domain of searching area. The higher power point at each step is assigned as the new center power point P_C for next step. The best perturbing duty cycle point D^*, which gives a global maximum power point P^*, can be finally found by reducing the domain of searching for each iteration.

3.1.3. *Peak bracketing with initial scanning (PBIS).* The peak bracketing with initial scanning (PBIS) algorithm is designed based on the combination of the DWS algorithm and the PB algorithm. The combination is aimed at reducing the cycle times to find the expected global maximum power point P^*. For the first phase, the DWS algorithm is used to find a new smaller size segmented domain of searching. Afterwards, the PB algorithm is used to bracket and find the best perturbing duty cycle point D^*, which gives a global maximum power point P^*.

3.2. **Simulation tools and configuration.**

3.2.1. *Simulation tools.* Another important tool in the MPPT research and development is the solar cell system modelling. Some works such as in [13, 19] and many others use a numerical computing software such as Matlab program or Simulink tool to model their solar cell system to investigate the characteristics of the solar cell system.

In our current paper, the combination of SPICE and a numerical computing software tool is used. The solar cell array and the DC/DC converter are firstly modelled in SPICE. The SPICE circuit model of the PV cells/arrays is equivalent with conventional crystalline-based PV cells [21]. Since SPICE is widely used by electronic manufacturers in industries, the computed powers, voltages and currents should approximate better the real conditions. The power curve characteristic (curve's slope, local and global maxima) of the solar array and the converter is then generated and transformed into power characteristic data that can be simulated using the numerical software tool. Our proposed MPPT algorithms are then used in the software tool to explore and analyze the performances of the proposed MPPT algorithms, i.e., decremented window-size scanning (DWS), peak bracketing (PB)

and PB with initial scanning (PBIS) are verified. Using the combination of the SPICE and the software tool, the simulation time can be shortened.

3.2.2. *Simulation configuration.* The diagram of the simulation setup is presented in Figure 3. The photovoltaic is arranged in 3×2 array (3 modules in series in 2 parallel paths). The solar modules are modelled in SPICE and each panel can be excited with changeable solar polar irradiance in W/m^2. The solar array parameters of the solar configuration are presented in Table 1. Although we select only the solar array with about 300 Wp, the solar array structure can be scaled up for larger power capacity. The selected solar array size is also moderate in terms of simulation time. Larger solar array capacity will result in larger SPICE simulation nodes and loops, which can lengthen simulation time. Moreover, the other important point is that the selected solar array structure is enough to configure several partial shading scenarios to test in simulations the proposed MPPT algorithms. The proposed MPPT algorithms can principally trace the global MPP on similar or almost similar power curve forms with smaller and larger power scales.

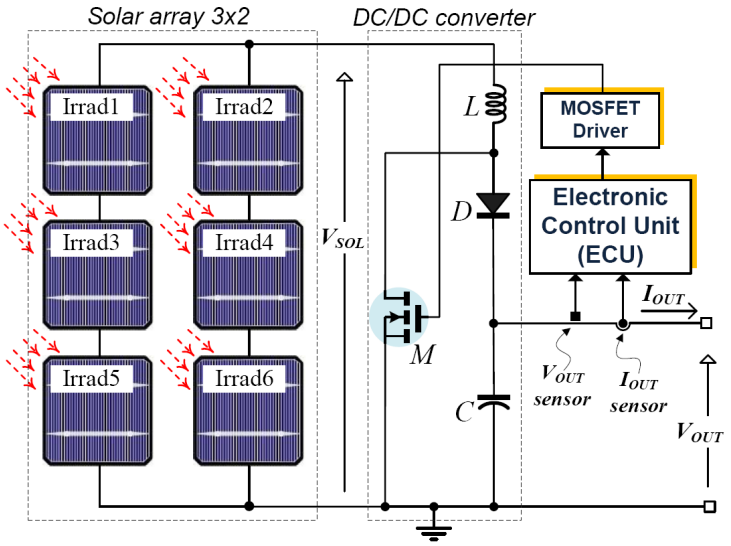

FIGURE 3. The simulation setup

TABLE 1. The specification data of the simulated solar array (3×2)

Solar Array Parameter	Values	Unit
Open Circuit voltage (V_{OC})	65.00352	Volt
Short Circuit Current (I_{SC})	6.1000	Ampere
Voltage at max. power (V_{mp})	51.9200	Volt
Maximum power (W_{mp})	302.7270	Watt
Current at max. power (I_{mp})	5.8307	Ampere

The variable irradiance values represent the partial shading conditions. Solar module having greater shading will have lower solar irradiance. The variation of this solar irradiance is then used to set up several partial shading scenarios as presented later in the simulation results (Section 4).

The P&O technique is equipped with a DC/DC converter besides an electronic control unit (ECU), where the MPPT algorithm is embedded on the ECU as shown in Figure 3. Some works or research articles such as in [20, 22] use a boost type DC/DC converter. We also use this converter type and the P&O technique in our work.

The boost-type DC/DC converter is used virtually to manipulate the output impedance of the photovoltaic systems in such a way that it will match the input impedance of the photovoltaic panel. The output impedance is manipulated by changing the duty cycle ratio of the pulse signal for the MOSFET's gate terminal. The MOSFET driver is used to drive the gate of the power MOSFET M. The inductance of the inductor L is 150 μH. The capacitance value of the electrolyte capacitor C is 220 μF.

4. **Simulation Results.** In this section, we simulate the power characteristic curves at the DC/DC converter output terminal for different resistance load parameter values. The power curves represent the relationships between the perturbing duty-ratios and the output power of the converter. Five scenarios, as presented in Table 2, are used to analyze the power characteristics, i.e., a scenario without partial condition, and four scenarios with different partial conditions. Certainly, there are so many possible partial conditions to configure. However, only a few conditions are selected, in which some of them have represented unique power characteristics with different local and global MPPs. For example, partial shading scenario 4 presents a partial shadow condition where the upper and lower parts of the solar array panel receive smaller non uniform solar irradiances. The scenario presents power curves with local and global MPPs.

Table 2. Partial condition scenarios for simulations

Shading Condition	Irrad1 W/m^2	Irrad2 W/m^2	Irrad3 W/m^2	Irrad4 W/m^2	Irrad5 W/m^2	Irrad6 W/m^2
No partial shading	1000	1000	1000	1000	1000	1000
Partial shading 1	200	500	1000	1000	400	1000
Partial shading 2	1000	300	400	1000	200	500
Partial shading 3	100	800	400	200	1000	500
Partial shading 4	300	200	800	1000	100	400

4.1. **Power points characteristics.** The following subsections present the power curves of five shading scenarios. The power curves are generated from perturbation of PWM signals modulated from 0 to 100% duty cycle for different resistance loads connected to the DC/DC converter output terminal.

The power characteristic curves of the DC/DC converter's output for the scenario without partial shading with different resistance load parameters is presented in Figure 4(a). It seems that power curves for load resistance values of 20Ω and 80Ω present local MPP.

Figure 4(b) presents the power characteristic curves of the DC/DC converter's output for the partial shading scenario 1 with different resistance load parameters. It seems that power curves for load resistance values of 10Ω, 20Ω, 30Ω and 40Ω present local MPP.

The power characteristic curves of the DC/DC converter's output for the partial shading scenario 2 with different resistance load parameters are shown in Figure 4(c). It seems that power curves for load resistance values of 20Ω, 30Ω and 40Ω present local MPP.

Figure 4(d) shows the power characteristic curves of the DC/DC converter's output for the partial shading scenario 3 with different resistance load parameters. It seems that power curve for load resistance value of only 10Ω presents local MPP.

The power characteristic curves of the DC/DC converter's output for the partial shading scenario 4 with different resistance load parameters are given in Figure 4(e). It seems that power curves for load resistance values of 20Ω, 30Ω, 40Ω, 60Ω, 80Ω and 100Ω present local MPP.

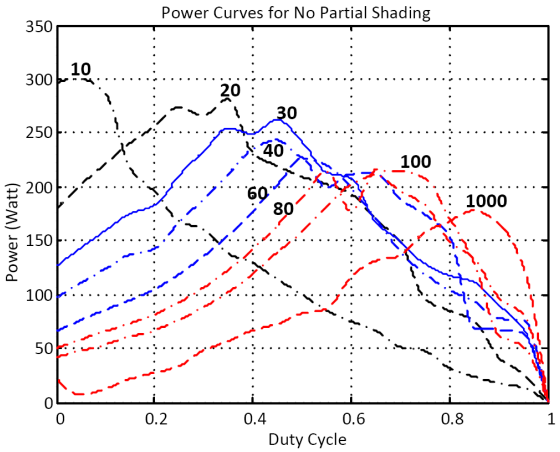

(a) No shading

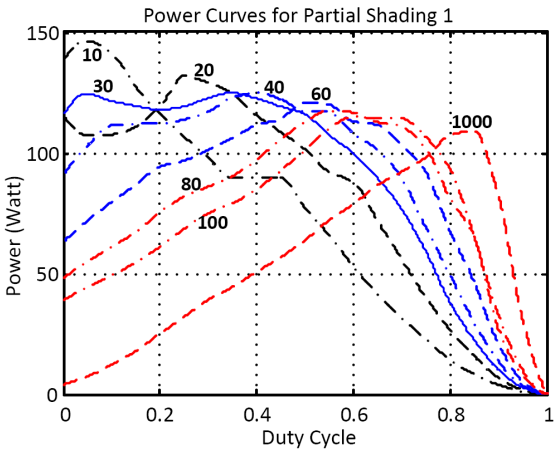

(b) Partial shading 1

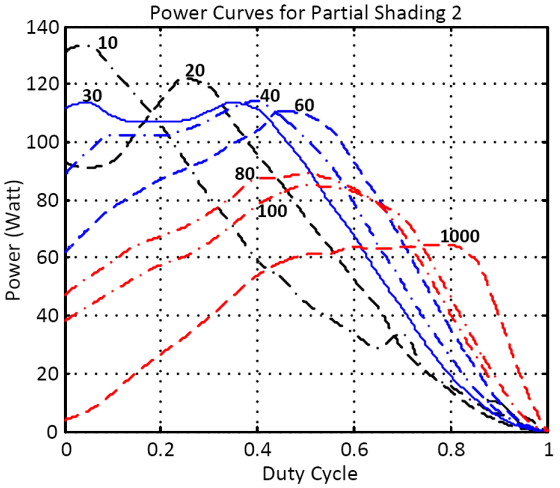

(c) Partial shading 2

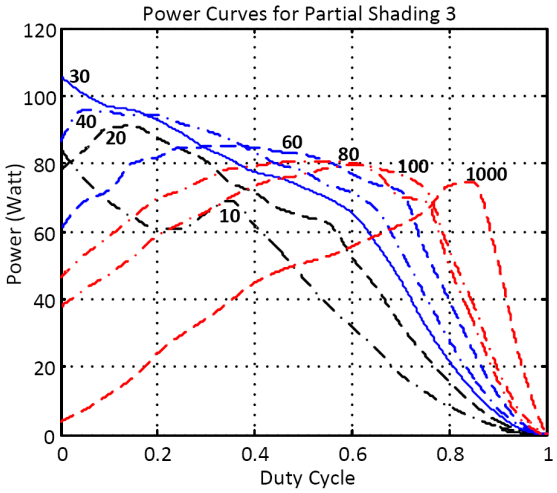

(d) Partial shading 3

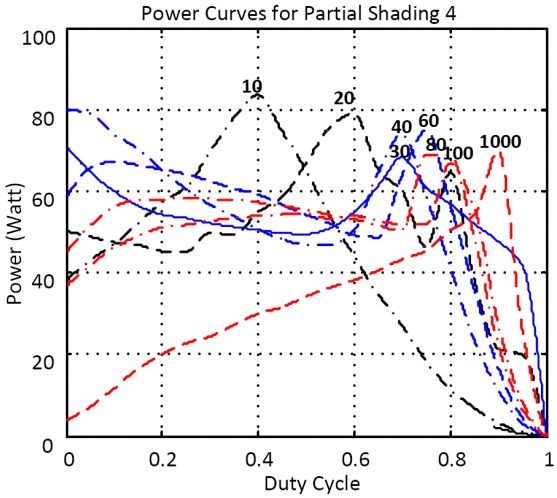

(e) Partial shading 4

FIGURE 4. Power characteristic curves of the DC/DC converter's output for five shading scenarios with different resistance load parameters

4.2. **Performance comparisons of the MPPT algorithms with load condition changes.** In this section, we will compare the performances of the three MPPT algorithms described before, under the five partial shading conditions that have been also explained before. The simulation is run in the following scenario. The algorithms are run for certain resistance load value. Then, when the algorithms converge into a certain power point, which is hopefully a global maximum power point, then the resistance load values is changed. Five resistance loads are used in the simulation scenarios, i.e., 10 Ω, 30 Ω, 60 Ω and 1 kΩ. Changes are made four times. For each resistance load value, each MPPT algorithm made about 40-50 perturbations-and-observation or P&O steps.

The duty cycle is set to 0.00 for 0.00% duty ratio, and 1.00 for 100.00% duty ratio. The digital duty ratio in decimal unit (decimal-coded digital duty ratio) is presented in tables at the consecutive figures. The decimal-coded digital duty ratio is used to simplify later the digital implementation of the algorithms. We assume that 10-bit digital duty ratio is used. Hence, 0.00% duty ratio is related to 0 decimal-coded digital value and 100.00% duty ratio is related to 1023 decimal-coded digital value.

Figure 5 presents the comparison between the MPPT algorithms to reach the maximum power point for the scenario without partial shadow. The DWS algorithm requires about (in average of) 42 P&O steps to reach the maximum power point. The PB algorithm requires about 26 P&O steps, while the PBIS needs about 41 P&O steps. The table on the right-hand side of the figure summarizes the reached steady-state points of the global MPPs with their related duty-ratio points using the proposed MPPT algorithms.

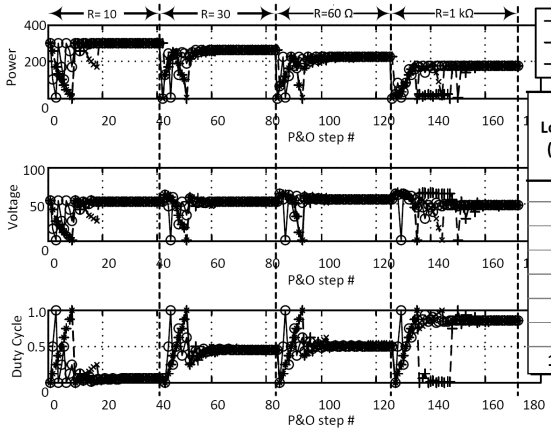

Load (Ω)	Decremented Window Scanning			Peak Bracketing (PB)			PB With Initial Scanning		
	Power (Watt)	Dig. Duty in Deci.	Duty Cycle	Power (Watt)	Dig. Duty in Deci.	Duty Cycle	Power (Watt)	Dig. Duty in Deci.	Duty Cycle
10	300.392	51	0.0498	300.392	51	0.0498	300.392	51	0.0498
20	281.1543	358	0.3496	274.1961	257	0.251	274.1961	257	0.251
30	262.5294	461	0.4502	262.5294	461	0.4502	262.5294	461	0.4502
40	243.3194	461	0.4502	243.3194	461	0.4502	243.3194	461	0.4502
60	225.873	512	0.5	225.873	512	0.5	225.873	512	0.5
80	215.4099	666	0.6504	215.4099	666	0.6504	215.4099	666	0.6504
100	210.6072	666	0.6504	210.6072	666	0.6504	210.6072	666	0.6504
1000	177.7048	870	0.8496	177.7048	870	0.8496	177.7048	870	0.8496

FIGURE 5. The computing iteration and the table for the last iteration values of the maximum power point tracing for condition without partial shading

Figure 6 presents the comparison between the MPPT algorithms to reach the maximum power point for partial shading scenario 1. The average P&O steps, that are required to reach the maximum power point, are almost the same as the results without partial shading. The reached steady-state points of the global MPPs with their related duty-ratio points using the proposed MPPT algorithms are summarized by the table on the right-hand side of the figure.

Figure 7 presents the comparison between the MPPT algorithms to reach the maximum power point for partial shading scenario 2. In this scenario, for the 30 Ω resistance load, the DWS and PBIS algorithms reach the maximum power point of 113.6696 W with duty cycle of 0.3994, while the PB algorithm reaches 113.572 W with duty cycle of 0.0498. It seems that the PB algorithm attains the local MPP, although this local MPP is slightly different from the global MPP, which is achieved by the DWS and PBIS algorithms. The

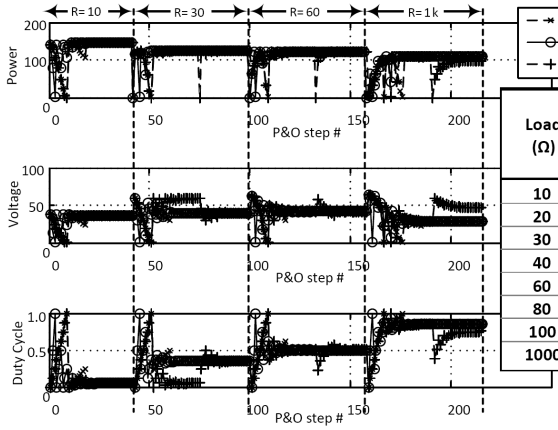

Load (Ω)	Decremented Window Scanning			Peak Bracketing (PB)			PB With Initial Scanning		
	Power (Watt)	Dig. Duty in Deci.	Duty Cycle	Power (Watt)	Dig. Duty in Deci.	Duty Cycle	Power (Watt)	Dig. Duty in Deci.	Duty Cycle
10	146.4459	51	0.0498	146.4459	51	0.0498	146.4459	51	0.0498
20	131.835	256	0.25	131.835	256	0.25	131.835	256	0.25
30	124.8868	358	0.3496	124.8868	358	0.3496	124.8868	358	0.3496
40	124.8457	410	0.4004	124.8457	410	0.4004	124.8457	410	0.4004
60	121.063	512	0.5	121.063	512	0.5	121.063	512	0.5
80	117.5419	563	0.5498	117.5419	563	0.5498	117.5419	563	0.5498
100	114.9918	615	0.6006	114.9918	615	0.6006	114.9918	615	0.6006
1000	109.1598	870	0.8496	109.1598	870	0.8496	109.1598	870	0.8496

FIGURE 6. The computing iteration and the table for the last iteration values of the maximum power point tracing for partial shading condition 1

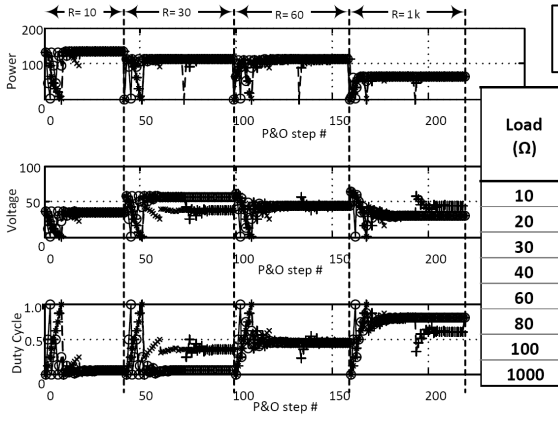

Load (Ω)	Decremented Window Scanning			Peak Bracketing (PB)			PB With Initial Scanning		
	Power (Watt)	Dig. Duty in Deci.	Duty Cycle	Power (Watt)	Dig. Duty in Deci.	Duty Cycle	Power (Watt)	Dig. Duty in Deci.	Duty Cycle
10	133.344	51	0.0498	133.344	51	0.0498	133.344	51	0.0498
20	122.083	256	0.25	122.083	256	0.25	122.083	256	0.25
30	113.6696	358	0.3496	113.572	51	0.0498	113.6696	358	0.3496
40	114.2095	409	0.3994	114.2095	409	0.3994	114.2095	409	0.3994
60	110.81	461	0.4502	110.81	461	0.4502	110.81	461	0.4502
80	89.128	512	0.5	89.128	512	0.5	89.128	512	0.5
100	84.958	521	0.5	84.958	521	0.5	84.958	521	0.5
1000	64.392	819	0.7998	64.392	819	0.7998	64.392	819	0.7998

FIGURE 7. The computing iteration and the table for the last iteration values of the maximum power point tracing for partial shading condition 2

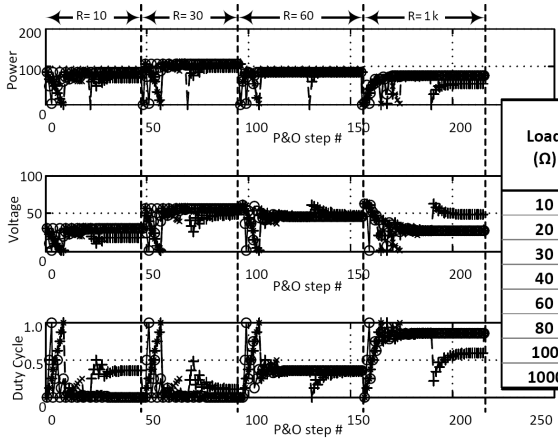

Load (Ω)	Decremented Window Scanning			Peak Bracketing (PB)			PB With Initial Scanning		
	Power (Watt)	Dig. Duty in Deci.	Duty Cycle	Power (Watt)	Dig. Duty in Deci.	Duty Cycle	Power (Watt)	Dig. Duty in Deci.	Duty Cycle
10	84.495	0	0	84.495	0	0	84.495	0	0
20	91.1069	153	0.1494	91.1069	153	0.1494	91.1069	153	0.1494
30	106.041	0	0	106.041	0	0	106.041	0	0
40	95.7768	51	0.498	95.7768	51	0.498	95.7768	51	0.498
60	85.3149	358	0.3496	85.3149	358	0.3496	85.3149	358	0.3496
80	80.671	512	0.5	80.671	512	0.5	80.671	512	0.5
100	79.6919	614	0.5996	79.6919	614	0.5996	79.6919	614	0.5996
1000	74.4229	870	0.8496	74.4229	870	0.8496	74.4229	870	0.8496

FIGURE 8. The computing iteration and the table for the last iteration of the maximum power point tracing for partial shading condition 3

table on the right-hand side of the figure summarizes the global MPPs with their related duty-ratio points reached using the proposed MPPT algorithms.

Figure 8 presents the comparison between the MPPT algorithms to reach the maximum power point for partial shading scenario 3. In this scenario, all of the MPPT algorithms

can reach the same global MPP. The reached steady-state points of the global MPPs with their related duty-ratio points using the proposed MPPT algorithms are summarized by the table on the right-hand side of the figure.

Figure 9 presents the comparison between the MPPT algorithms to reach the maximum power point for partial shading scenario 4. For the 60 Ω resistance load, the DWS and PBIS algorithms reach the maximum power point of 74.915 Watt with duty cycle of 0.75, while the PB algorithm reaches 67.3468 W with duty cycle of 0.0996. It seems that the PB algorithm attains the local MPP, which is quite large (about 7.5682 W) compared to the global MPP achieved by the DWS and PBIS algorithms. The table on the right-hand side of the figure summarizes the steady-state points of the global MPPs with their related duty-ratio points, which are reached using the proposed MPPT algorithms.

4.3. **Performance comparisons of the MPPT algorithms with runtime shading condition changes.** In this subsection, the MPPT algorithms are tested with the

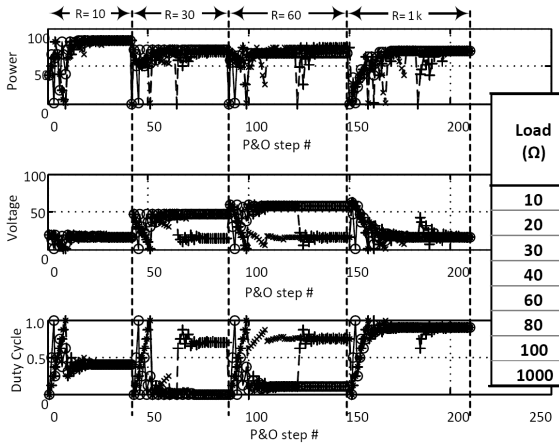

Load (Ω)	Decremented Window Scanning			Peak Bracketing (PB)			PB With Initial Scanning		
	Power (Watt)	Dig. Duty in Deci.	Duty Cycle	Power (Watt)	Dig. Duty in Deci.	Duty Cycle	Power (Watt)	Dig. Duty in Deci.	Duty Cycle
10	83.5719	410	0.4004	83.5719	410	0.4004	83.5719	410	0.4004
20	79.0937	614	0.5996	79.0937	614	0.5996	79.0937	614	0.5996
30	71.139	0	0	71.139	0	0	71.139	0	0
40	80.03	0	0	80.03	0	0	80.03	0	0
60	74.915	768	0.75	67.3468	102	0.0996	74.915	768	0.75
80	68.838	768	0.75	68.838	768	0.75	68.838	768	0.75
100	54.467	512	0.5	54.467	512	0.5	54.467	512	0.5
1000	69.8164	921	0.8994	69.8164	921	0.8994	69.8164	921	0.8994

FIGURE 9. The computing iteration and the table for the last iteration values of the maximum power point tracing for partial shading condition 4

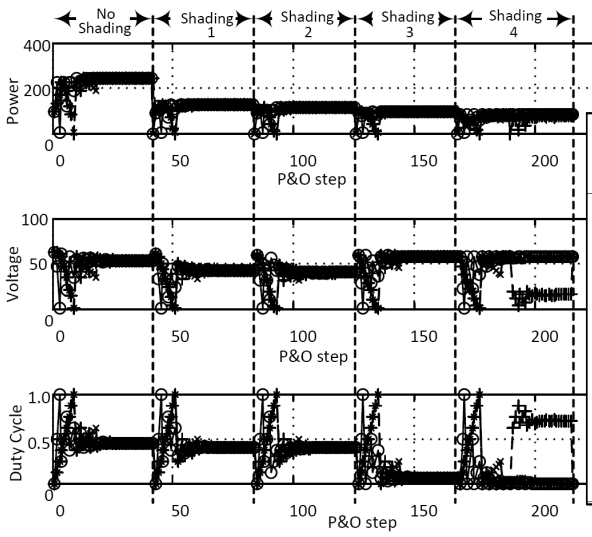

Partial Shading Scenario	Decremented Window Scanning			Peak Bracketing			Peak Bracketing With Initial Scanning		
	Power (Watt)	Dig. Duty in Deci.	Duty	Power (Watt)	Dig. Duty in Deci.	Duty	Power (Watt)	Dig. Duty in Deci.	Duty
Without Partial Shading	243.3194	461	0.4502	243.3194	461	0.4502	243.3194	461	0.4502
Partial Shading 1	124.8457	410	0.4004	124.8457	410	0.4004	124.8457	410	0.4004
Partial Shading 2	114.2095	409	0.3994	114.2095	409	0.3994	114.2095	409	0.3994
Partial Shading 3	95.7768	51	0.498	95.7768	51	0.498	95.7768	51	0.498
Partial Shading 4	80.03	0	0	80.03	0	0	80.03	0	0

FIGURE 10. The computing iteration and the table for the last iteration values of the maximum power point tracing for fixed loading with shading condition changes

changes of shading conditions at runtime. As presented before, there are five benchmarked shading conditions. During the simulation run, shading condition is changed in every about 40 until 50 P&O steps. Figure 10 shows the simulation results. The table on the right-hand side of the figure summarizes the steady-state points of the reached MPPs using the MPPT algorithm. As shown in the figure, all tested MPPT algorithms can reach the same global MPPs with also the same duty-ratio perturbations.

Measurement values of the number of P&O steps required to reach the steady-state global MPPs depend on the shading and loading conditions. However, from some simulation results, these values can be estimated in average. Table 3 summarizes the measured values for 4 different P&O-based MPPT algorithms. We can see that the PBIS MPPT algorithm presents the best minimum average P&O steps (about 26 P&O steps in average) to reach the global MPPs.

TABLE 3. The average performance comparisons between 4 P&O MPPT algorithms

P&O Algorithm	Hill Climbing	DWS	PB	PBIS
Averg. Numb. of P&O steps	259	42	26	38

The simulation results have presented that, for some partial shading conditions, the proposed MPPT algorithms presented almost similar performance. In some cases, they can trace the maximum power points, even when the parameter values of the resistance loads change during simulation runtime. However, there are still some different results achieved by using the PB algorithm. The PB algorithm reaches a local MPP for a few case.

In terms of accuracy, the DWS and PBIS algorithms present better performance compared to the PB algorithm. However, in terms of speed, the PB algorithm presents the best results. It requires about 26 P&O steps in average to reach the MPP using the PB algorithm. The DWS algorithm requires about 42 in average to reach the global MPP. Meanwhile, the PBIS algorithm can achieve the global MPP by making about 38 P&O steps for its best performance. We must note that the minimum number of P&O steps to reach global MPP can be different depending on the forms of power curves, such as the curve slope and the number of local MPP appearing on the curves. In general, the proposed MPPT algorithms highly outperform the P&O hill-climbing algorithm. Table 3 presents the average number of P&O steps required to reach the global MPPs for the traditional hill-climbing algorithm and our proposed algorithms.

5. **Conclusions.** This paper has presented three proposed P&O MPPT algorithms, which operate based on iterative power point scanning technique. The boost-type DC/DC converter is used to control the solar system operating at its maximum power point, where the reference power is measured at the DC/DC converter output terminal. The maximum power points of the power curves measured from the solar array output and the converter output terminals are not always at the same duty cycle point. The power measurement should be done from the converter output, because this power is more actual for the users point of view. Additionally, the current at the solar array output terminal has ripple whose frequency is high and equal to the switching frequency for the used DC/DC converter. This ripple is not good for long term current sensor operations, can shorten the sensor lifetime and induce extra switching power loss at the sensor.

The main advantageous characteristic of our MPPT algorithms is the need for small number of iterative P&O steps to reach global MPP, resulting in a small computing delay. When a hardware implementation needs 1 μs to finish one P&O step, then, with 38 P&O steps, the PBIS MPPT algorithm could reach a global MPP about 38 μs in average, a

small computing delay value. Thus, the iterative scanning-based MPPT algorithms can be further embedded in a microcontroller or FPGA device with relatively low computing energy demand due to the small size of computing iteration.

The other advantageous features of our proposed MPPT algorithms are their ability to respond the rapid changes of partial shading and load conditions, as well as their independence from solar technologies. When a new solar array with different technologies is installed, we do not need to reconfigure algorithms or to re-train the algorithms like fuzzy logic, neural network or AI methods [6, 8]. The only thing to do is to scale up/down properly the voltage/current measurements such that the sensed signals can be calibrated and further processed well.

Acknowledgment. The authors gratefully acknowledge the Ministry of Research, Technology and Higher Education of the Republic of Indonesia for funding our research work under the scheme of "Post-Graduated Colleagium Research Grant" (*Hibah Penelitian Tim Pasca Sarjana*) with Grant Contract No. 005/SP2H/LT/DPRM/IV/2017 in the year 2017.

REFERENCES

[1] M. A. Elgendy, B. Zahawiand and D. J. Atkinson, Operating characteristics of the P&O algorithm at high perturbation frequencies for standalone PV systems, *IEEE Trans. Energy Conversion*, vol.30, no.1, pp.189-198, 2015.

[2] N. Femia, G. Petrone, G. Spagnuolo and M. Vitelli, Optimization of perturb and observe maximum power point tracking method, *IEEE Trans. Power Electronics*, vol.20, no.4, pp.963-973, 2005.

[3] P. Lei, Y. Li and J. E. Seem, Sequential ESC-based global MPPT control for photovoltaic array with variable shading, *IEEE Trans. Sustainable Energy*, vol.2, no.3, pp.348-358, 2011.

[4] J. Ma, K. L. Man, T. O. Ting, N. Zhang, C.-U. Lei and N. Wong, A hybrid MPPT method for photovoltaic systems via estimation and revision method, *Proc. of the IEEE Int'l Symp. on Circuits and Systems (ISCAS)*, pp.241-244, 2013.

[5] B. Veerasamy, W. Kitagawa and T. Takeshita, MPPT method for PV modules using current control-based partial shading detection, *Proc. of the Int'l Conf. on Renewable Energy Research and Application (ICRERA)*, pp.359-364, 2014.

[6] T. Esram and P. L. Chapman, Comparison of photovoltaic array maximum power point tracking techniques, *IEEE Trans. Energy Conversion*, vol.22, no.2, pp.439-449, 2007.

[7] K. Dahech, M. Allouche, T. Damak and F. Tadeo, Backstepping sliding mode control for maximum power point tracking of a photovoltaic system, *Electric Power Systems Research*, vol.143, pp.182-188, 2017.

[8] B. Subudhi and R. Pradhan, A comparative study on maximum power point tracking techniques for photovoltaic power systems, *IEEE Trans. Sustainable Energy*, vol.4, no.1, pp.89-98, 2013.

[9] S. L. Brunton, C. W. Rowley, S. R. Kulkarni and C. Clarkson, Maximum power point tracking for photovoltaic optimization using ripple-based extremum seeking control, *IEEE Trans. Power Electronics*, vol.25, no.10, pp.2531-2540, 2010.

[10] L. Jiang and D. L. Maskell, A simple hybrid MPPT technique for photovoltaic systems under rapidly changing partial shading conditions, *Proc. of the 40th Photovoltaic Specialist Conference (PVSC)*, pp.782-787, 2014.

[11] J. Ahmed and Z. Salam, An improved method to predict the position of maximum power point during partial shading for PV arrays, *IEEE Trans. Industrial Informatics*, vol.11, no.6, pp.1378-1387, 2015.

[12] S. Mohanty, B. Subudhi and P. K. Ray, A new MPPT design using grey wolf optimization technique for photovoltaic system under partial shading conditions, *IEEE Trans. Sustainable Energy*, vol.7, no.1, pp.181-188, 2016.

[13] A. Sandali, T. Oukhoya and A. Cheriti, Modeling and design of PV grid connected system using a modified fractional short-circuit current MPPT, *Proc. of the Int'l Renewable and Sustainable Energy Conf. (IRSEC)*, pp.224-229, 2014.

[14] M. Kermadi and E. M. Berkouk, Artificial intelligence-based maximum power point tracking controllers for photovoltaic systems: Comparative study, *Renewable and Sustainable Energy Reviews*, vol.69, pp.369-386, 2017.

[15] P. Konghuayrob and S. Kaitwanidvilai, Maximum power point tracking using hybrid fuzzy based P&O and back propagation (BP) neural network for photovoltaic system, *International Journal of Innovative Computing, Information and Control*, vol.10, no.5, pp.1949-1960, 2014.
[16] R. Boukenoui, H. Salhi, R. Bradai and A. Mellit, A new intelligent MPPT method for stand-alone photovoltaic systems operating under fast transient variations of shading patterns, *Solar Energy*, vol.124, pp.124-142, 2016.
[17] A. Borni, T. Abdelkrim, N. Bouarroudj, A. Bouchakour, L. Zaghba, A. Lakhdari and L. Zarour, Optimized MPPT controllers using GA for grid connected photovoltaic systems: Comparative study, *Energy Procedia*, vol.119, pp.278-296, 2017.
[18] S. K. Kollimalla and M. K. Mishra, Variable perturbation size adaptive P&O MPPT algorithm for sudden changes in irradiance, *IEEE Trans. Sustainable Energy*, vol.5, no.3, pp.718-728, 2014.
[19] M. Sameeullah and A. Swarup, Modeling of PV module to study the performance of MPPT controller under partial shading condition, *Proc. of the IEEE 6th India Int'l Conf. on Power Electronics (IICPE)*, pp.1-6, 2014.
[20] Y.-H. Wang, W.-C. Liu and T.-H. Kuo, A 200W MPPT boost converter for BIPV applications with integrated controller, *Proc. of the Int'l Symp. on Computer, Consumer and Control*, pp.288-291, 2014.
[21] Syafaruddin, F. A. Samman, Alfian, M. A. Idris, S. H. Ahsan and S. Latief, Characteristics approach of thin film CIGS PV cells with conventional Mono-Christalline silicon model, *International Journal of Innovative Computing, Information and Control*, vol.12, no.1, pp.171-180, 2016.
[22] P. Sanjeevikumar, G. Grandi, P. W. Wheeler, F. Blaabjerg and J. Loncarski, A simple MPPT algorithm for novel PV power generation system by high output voltage DC-DC boost converter, *Proc. of the 24th IEEE Int'l Symp. on Industrial Electronics (ISIE)*, pp.214-220, 2015.